

Excluded-volume interactions and structure formation in monolayers of bent-core systems.

Lech Longa¹, Paweł Karbowniczek², Michał Cieśla¹ and Agnieszka Chrzanowska²

¹*Marian Smoluchowski Institute of Physics,
Department of Statistical Physics and Mark
Kac Center for Complex Systems Research,
Jagiellonian University,
ul. Łojasiewicza 11,
30-348 Kraków, Poland*

*Institute of Physics,
Kraków University of Technology,
ul. Podchorążych 1,
30-084 Kraków, Poland.*

Abstract

Two-dimensional assemblies of bent-core shaped molecules attain at highly orienting surfaces liquid crystalline structures characteristic mostly for lamellar chiral or nonchiral antiferroelectric order. Here, using the Onsager-type of density functional theory we investigate the role of excluded-volume interactions in stabilizing different structures in monolayers filled with bent-shaped molecules. We study influence of molecular features, like the apex angle, thickness of the arm and the type of the arm edges on the stability of layered structures. For molecular shapes taken the observed phases are dominated by the lamellar antiferroelectric type as observed experimentally, but a considerable sensitivity of the ordering to details of the molecular shape is found for order parameters and wave vectors of the structures. Interestingly, for high packing fractions smectic A, ferroelectric smectic A and ferroelectric nematic phases are foreseen from the bifurcation analysis and explicit free energy minimization. The presented theory models equilibrium properties of bent-core liquid crystals subjected to strong planar anchoring, *i.e.* in the case when details of the surface are of secondary importance.

PACS 64.70.mf Theory and modeling of specific liquid crystal transitions, including computer simulation PACS 61.30.Cz Molecular and microscopic models and theories of liquid crystal structure PACS 05.20.Jj Statistical mechanics of classical fluids

I. INTRODUCTION

Two-dimensional structures made by complicated macromolecules are recently of great interest due to their potential applications, mainly in photoelectronic and biosensor area [1–8]. In contrast to assemblies of spherical objects like, for instance, colloidal or nanosilica spheres, in case of anisotropic or irregularly shaped particles, there is a possibility to realize monolayers exhibiting very regular patterns which, next, can be utilized as a matrix capable to orient liquid crystal or to fabricate elements of electronic devices [5]. It has also turned out that the structure of a matrix built within a monolayer may influence the activity of biomolecules. This biomolecular effect is a first step for biosensors construction. A comprehensive and detailed report about ordered molecular assemblies formed by Langmuir Blodgett films and self-assemblies with potential influence on biosensing capabilities is given in [2].

Achiral bent-core (banana) shaped molecules can be important in this regard [1, 3–5, 9, 10]. This arises from the observation of extraordinary selforganization in these mesogens in 3D, like the twist-bent nematic phase of nanoscale pitch [11, 12], the fibre forming smectic twist-bent phase [13] and the cybotactic nematic phase [14]. They are also promising candidates to form the elusive biaxial nematic phase [15] and even more complex structures with tetrahedric order [16, 17].

In 2D the situation is more subtle. These systems are generally characterized by the lack of true long range order in the nematic state, which is a consequence of director's fluctuations. A continuous nematic-isotropic phase transition goes here via Kosterlitz-Thouless disclination unbinding mechanism yielding what is observed as algebraically decaying orientational pair correlation function in the nematic phase [18]. It is observed, for example, in simulations of a 2D system of hard needles with zero thickness [19, 20], for planar hard rods [21] and for zig-zag and bow-shaped hard needles [22]. Even though the true long-range nematic order does not exist in these systems on a macroscopic scale the simulations show

that it persists over large spatial dimensions (*i.e.* on a mesoscopic scale). Interestingly, it can be well described by means of the Onsager's Density Functional Theory (DFT) [23], despite the fact that macroscopic fluctuations of the director are generally not included in DFT.

On the experimental side the data of Gong and Wan [1] for banana-shaped liquid crystal molecules (P-n-PIMB) deposited on a highly orienting pyrolytic graphite (HOPG) surface reveal that the nematic order can be nearly saturated over the sample. Using scanning tunneling microscopy (STM) the authors observed here several antiferroelectric chiral and nonchiral lamellar structures. Other nanostructure assemblies with local polarization - domains, rings or spirals - are also reported in literature [3, 4].

Antiferroelectric smectic order in dense 2D banana systems has been also discussed theoretically as prevailing in [24] by Bisi *et al.* based on the packing arguments and, later, by Gonzales *et al.* in the case of needle-like, infinitely thin boomerangs [25] and hockey stick-shaped molecules consisting of two line segments [26]. It has been also detected in zero-thickness zig-zag and bow-shaped systems [22]. In addition, in [25, 26] the authors have observed that upon increasing pressure, before the system attains antiferroelectric smectic A phase, a spatially non-uniform, bend-deformed nematic structure is being formed, which consists of orientationally ordered polar domains with the overall zero net polarization. Similar, but much better ordered, modulated nematic order with bend-like deformations has also been reported for bow-shaped molecules [22].

Understanding molecular self-organization in thin layers of more realistic, *finite-thickness* bent-core molecules is an interesting theoretical issue. Since most studies on two-dimensional systems are based on the particles exhibiting geometrical shapes like needles [19, 23], hard discorectangles [27], or zigzag particles [28] interacting via hard core potentials, we will also incorporate a model from this class (it will be discussed in detail later). Both types of approach - the performed so far MC simulations and Onsager's Density Functional Theory (DFT) - give consistent predictions here. Of particular importance on the phase stabilization are excluded volume effects due to primary molecular features of the particles. In the case of bananas these features are: length and width of the arms and the apex angle. As it will be shown, the secondary features like *e.g.* the shape of the arm's end can also prove important.

As already mentioned above the DFT of Onsager's type has proven to give a good insight into qualitative features of the phases. One of the benefits of using the DFT scheme in

connection with bifurcation and symmetry analyses is the fact that it allows to cover a broad range of cases giving clear directions for a more detailed study. The theory predicts the existence of the ordered mesophases with weakly first or second-order phase transitions in 2D systems, and hence cannot predict quasi long-range order (QLRO), which is characteristic for systems with a continuous broken symmetry. Even though the Onsager's DFT does not account for QLRO, it works surprisingly well for nonseparable, hard body interactions [23]. Indeed, a comparison of the Onsager DFT and MC predictions suggest that the former theory is able to account for relevant features of molecular selforganization [19, 22, 23, 25, 28].

The aim of the present paper is to investigate with the Onsager's DFT a possibility of structure formation in monolayers built from hard bent-core molecules of finite thickness. In particular we show that even a small change in molecular shape can have a profound effect on the properties and even stability of the structures. We limit ourselves to the case of high orientational order, in agreement with experiment [1] and previous 2D studies [25].

The paper is organized as follows: Section II presents the model and Section III introduces the Onsager's DFT formalism together with the appropriately identified order parameters, needed for the structure description of aligned boomerangs. Section IV gives the results of the bifurcation analysis for the lamellar structures. Section V provides exemplary phase diagrams obtained from the full minimization for three different bent-core systems: hard needle-like bananas, finite thickness bananas with flat horizontal edges and finite thickness bananas with squared edges. Finally, in the last section a summary is given together with the main conclusions.

II. MODEL

We are going to study molecular selforganization in a two-dimensional system of hard bent-core molecules of finite thickness. Three types of the molecules will be studied: needle-like boomerangs, Fig.(1a), finite thickness boomerangs with horizontally cut edges (HB), Fig.(1b), and finite thickness boomerangs with squared edges (SB), Fig.(1c).

The bent core needles, which are the reference particles given in Fig.(1a), are just two line segments of the length l joined at one end in such a way that they form the apex angle of 2ψ . To obtain a HB molecule the line segments are replaced by rhomboids whose tilt angle conforms to the assumption that the edges are effectively horizontal as in Fig.(1b).

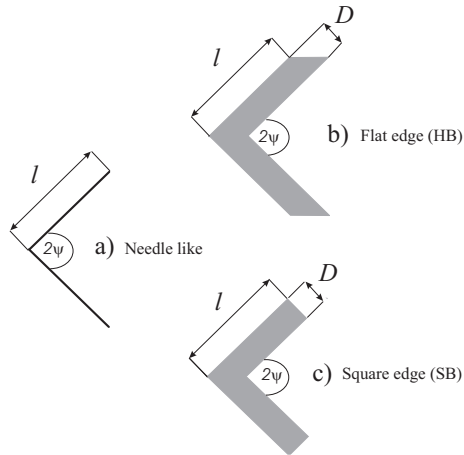


FIG. 1: Shapes of bent-core molecules studied: (a) bent-core needles (they serve as a reference), (b) finite thickness bent-core molecules with flat horizontal edges (HB), and (c) finite thickness bent-core molecules with squared edges (SB). The apex angle, ψ , is here $\pi/4$ and the arm's width is $D = l/4$.

The SB molecules will differ from the HB molecules with respect to the shape of the arm edges, which in the SB case are squared. D describes here the arm's thickness.

We should add that we sought for several possibilities of introducing finite thickness to needle-like boomerangs. The SB molecules seem to be the most natural extension, whereas boomerangs with horizontally cut arms (the HB particles) are expected to attain a layered arrangement more easily. Importantly, for all three cases the excluded areas can be calculated analytically. As it will be seen later, this slight change in the arm's shape of the particles can substantially influence the equilibrium properties of the system, especially for higher packing fractions.

In order to compare the results for these three differently shaped bananas, Fig.(1), we introduce the dimensionless shape parameter $\delta = D/l$ ($0 \leq \delta \lesssim 1$) and define the reduced density

$$\rho = \bar{\rho} l^2 \sin(2\psi), \quad (1)$$

where $\bar{\rho} = N/S$ stands for the average density with N being the number of particles within the surface area S . Using definition of the packing fraction parameter $\eta_{mol} = NS_{mol}/S$, with

S_{mol} being the surface of the molecule, the reduced density becomes

$$\rho = \eta_{mol} \frac{l^2 \sin(2\psi)}{S_{mol}}. \quad (2)$$

In the case of the HB particles, $S_{mol} = 2l^2\delta$. Thus

$$\rho = \eta_{mol} \frac{\sin(2\psi)}{2\delta}. \quad (3)$$

For the SB particles $S_{mol} = l^2\delta(2 - \delta/\tan(\psi))$. Then

$$\rho = \eta_{mol} \frac{\sin(2\psi)}{\delta(2 - \delta/\tan(\psi))}. \quad (4)$$

Please note that the parametrization (2) is singular for $\psi = 0$ and $\psi = \pi/2$, where bent-core molecules of zeroth thickness become reduced to a line. For 3D liquid crystals the typical packing fractions accessible to liquid crystalline phases attain values from the interval (0.4-0.7). These numbers can go to even higher values in 2D as observed for lamellar structures in experiments of Gong and Wan [1]. For our HB and SB boomerangs the packing fraction can reach its maximal possible value of $\eta_{mol} = 1$ for ideal, close-packed, lamellar configurations with maximally polarized layers.

III. DENSITY FUNCTIONAL ANALYSIS

A. Free energy and self-consistency equations

The simplest formula describing the phase behavior of hard-body liquid crystalline systems is the Onsager's low-density free energy functional obtained within second virial approximation [29]

$$\begin{aligned} \mathcal{F}[\rho] = & k_B T \operatorname{Tr}_{(X)} \{ \rho(X) [\ln(\Lambda\rho(X)) - 1] \} + \operatorname{Tr}_{(X)} [\rho(X) V_{ext}] \\ & - \frac{k_B T}{2} \operatorname{Tr}_{(X_1, X_2)} [\rho(X_1) f_{12} \rho(X_2)], \end{aligned} \quad (5)$$

where

$$f_{12} = e^{-\beta V(X_1, X_2)} - 1 \quad (6)$$

is the Mayer function. Here V is the interparticle potential, V_{ext} is the external potential, representing interaction with external fields, or surfaces, Λ is the constant resulting from the integration over momenta, T is the absolute temperature and k_B is the Boltzmann constant. $\rho(X)$ stands for the one-particle distribution function, which is normalized to the total number of particles N

$$\text{Tr}_{(X)}[\rho(X)] = \langle N \rangle \equiv N. \quad (7)$$

In what follows no external fields are taken into account and the surface is assumed smooth at the lengthscale of the molecular size (typically a few nanometers for bent-core molecules). Its role is limited to confine molecules in 2D (strong planar anchoring). Under these assumptions the corresponding V_{ext} does not depend on molecular orientational degrees of freedom and, hence, can be disregarded in the expansion (5).

The variable X represents the set describing the position $\mathbf{r} = (x, y)$ of the center of mass of the particle and its orientations. In the description of lamellar structures we assume, in agreement with experiment [1] and previous 2D studies [25], that orientational order is nearly saturated. In practice it means that for a C_{2h} -symmetric molecule the orientational degrees of freedom become reduced to a discrete variable, say s , accounting only for two possible orientations of the steric dipole ($s = \pm 1$) with respect to the director \mathbf{n} , where $s = +1$ denotes a particle with a steric dipole pointing to the right and $s = -1$ denotes a particle with a dipole pointing to the left. In what follows we limit orientational degrees of freedom of a molecule to the above two values. In addition, if not stated otherwise, we assume that the steric dipole is perpendicular to the (local) director, Fig.(2). Hence, in 2D

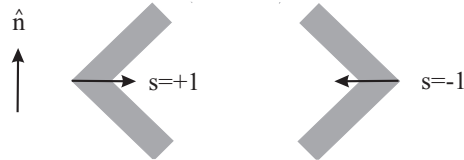


FIG. 2: Definition of s variable, accounting for different orientations of molecule's steric dipole with respect to the local director.

the trace in Eqs. (5,7) is calculated as

$$\begin{aligned} Tr_{(X)} &= \sum_{s=\pm 1} \int_0^L dx \int_0^L dy = \\ &S \sum_{s=\pm 1} \frac{1}{L} \int_0^{Md=L} dy, \end{aligned} \quad (8)$$

where L represents the linear dimension of our sample ($S = L^2$); M stands for the number of layers and d is the layer thickness in the case of smectics.

In order to obtain the equilibrium solutions for the distribution function the free energy functional $\mathcal{F}[\rho]$ must be minimized with respect to variation of $\rho(X)$ subject to the normalization constraint $Tr_{(X)}[\rho(X)] = N$. It amounts in minimizing $\mathcal{F}^*[\rho]$ given by

$$\mathcal{F}^*[\rho] = \mathcal{F}[\rho] - \mu \left\{ Tr_{(X)}[\rho(X)] - N \right\}, \quad (9)$$

where μ is the chemical potential. In our case of ideally oriented hard boomerangs the Mayer function has a meaning of an excluded distance. It reads

$$f_{12} = e^{-\beta V(X_1, X_2)} - 1 = -\Theta[\xi(\hat{\mathbf{r}}_{12}, s_1, s_2) - r_{12}], \quad (10)$$

where $\hat{\mathbf{r}}_{12} = \frac{\mathbf{r}_{12}}{r_{12}} = \frac{\mathbf{r}_2 - \mathbf{r}_1}{|\mathbf{r}_2 - \mathbf{r}_1|}$ and ξ is the contact function defined as the distance of contact from the origin of the second molecule for a given direction $\hat{\mathbf{r}}_{12}$ and orientations s_1, s_2 (see Fig. (3)); Θ denotes the Heaviside function. Now, introducing the probability distribution function $P(X)$

$$\rho(X) = NP(X) = \bar{\rho}SP(X), \quad (11)$$

and disregarding irrelevant (constant) terms, one can rewrite the free energy (5) in terms of a rescaled free energy per unit area, $f(P)$, as

$$\begin{aligned} \frac{f(P)}{l^2 \sin(2\psi)} &= \frac{\beta \Delta \mathcal{F}[P]}{S} = \\ &\bar{\rho} Tr_{(X)} [P(X) \ln P(X)] + \frac{\bar{\rho}}{2} Tr_{(X)} [P(X) H_{eff}(X)], \end{aligned} \quad (12)$$

where H_{eff} is the effective excluded volume, averaged over probability distribution of particle

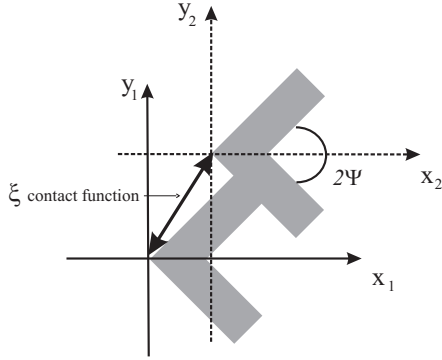


FIG. 3: Definition of the contact function ξ for two molecules with the apex angle $2\psi = \pi/2$ and $\delta = D/l = 1/3$.

”2”. It reads

$$H_{eff}(X_1) = \bar{\rho} S Tr_{(X_2)} \{P(X_2) \Theta [\xi(X_1, X_2) - r_{12}]\}. \quad (13)$$

The equilibrium distribution function is now obtained by minimizing the free energy functional (12). The necessary condition reads

$$\frac{\delta f(P)}{\delta P} = 0, \quad (14)$$

which in practice becomes reduced to solving the self-consistent nonlinear integral equations for $P(X)$

$$P(X) = Z^{-1} e^{-H_{eff}(X)}, \quad (15)$$

where

$$Z = Tr_{(X)} e^{-H_{eff}(X)} \quad (16)$$

is the normalization of $P(X)$. The stationary solution of Eq. (15) will be denoted $P_s(X)$.

Before we carry out the explicit calculations it is important to realize that the low-density, Onsager’s approximation is quantitatively poor for nematic and lamellar structures. In case of smectics, even inclusion of higher-order virial coefficients does not make quantitative agreement satisfactory. As it turns out, quantitatively correct results can still be obtained from the Onsager’s theory by following the Parsons-Lee (PL) rescaling/resummation technique [30, 31]. They showed that the effect of (infinite) hierarchy of higher-order virial terms can partly be taken into account in (12) by an appropriate renormalization of the second

virial coefficient.

Effectively, the PL rescaling replaces the second-order virial packing fraction, η , entering Eq. (12) through $\bar{\rho} = \eta/S_{mol}$, by a renormalized packing fraction, which is a monotonic function of η_{mol} . The PL procedure, developed essentially for 3D systems, has been extended to 2D by Varga and Szalai [32]. One possibility, shown to work well at least for convex molecules, is equivalent to the replacement

$$\eta \rightarrow \frac{1}{2} \left(\frac{\eta_{mol}}{1 - \eta_{mol}} - \log(1 - \eta_{mol}) \right). \quad (17)$$

That is, the physical range of $\eta_{mol} \leq 1$ is mapped effectively on the infinite region of $\eta \geq 0$. Assuming, for example, $\eta_{mol} \lesssim 0.8$ would be equivalent to substitute $\eta \lesssim 2.8$ in (12). Such rescaling of the free energy quantitatively improves the predictions of Onsager's theory but does not *qualitatively* affect the sequence of phases and order of phase transitions. Therefore, in what follows, we leave Onsager's η to parameterize our results, but permit $\eta > 1$ in agreement with (17).

B. Details of the calculation

In the analysis of stable phases we disregard crystalline structures. Thus, for the case of perfectly aligned boomerangs only two variables are needed to parameterize one particle distribution function, say the vertical coordinate y and the orientational state $s = \pm 1$ of the particle, representing two opposite orientations of the steric dipole with respect to the director. Hence

$$P(X) \equiv P(s, y). \quad (18)$$

First, we will identify the bifurcation points from the perfectly ordered reference nematic phase. The relevant structures which can occur are commensurate or incommensurate smectics of A or C type, polar nematics and phases with splay-bend characteristics.

For the cases not involving nematic splay-bend structures [33, 34] the distribution function

can be Fourier-expanded as

$$P(s, y) = \tilde{A}_0 + \sum_{n=1}^{\infty} \tilde{A}_n \cos\left(\frac{2\pi ny}{d} - \phi_{0,n}\right) + s \tilde{B}_0 + \sum_{m=1}^{\infty} s \tilde{B}_m \cos\left(\frac{2\pi my}{d'} - \phi_{1,m}\right), \quad 0 \leq y \leq L, \quad (19)$$

where periodic boundary conditions are assumed: $L = Md = M'd'$, with $M > 0$ and $M' > 0$ being integer numbers.

Note that the expansion (19) is the most general representation for $P(s, y)$, subject to periodic boundary conditions. It follows from the observation that $P(s, y)$, where $s = \pm 1$, is linear in s : $P(s, y) = \tilde{A}(y) + s\tilde{B}(y)$. Consequently, the independent Fourier expansions of $\tilde{A}(y)$ and $\tilde{B}(y)$ involve the density wave part (\tilde{A}_n -terms) and the polarization wave part (\tilde{B}_n -terms) of periodicities d and d' , respectively. They are phase-shifted with respect to each other (ϕ phases), where the phases are determined up to a global phase, expressing freedom in choosing the origin of laboratory system of frame.

Using orthogonality properties of the Fourier series and properties of the s-space we can now define order parameters. They are given by

$$\begin{aligned} \langle x_n \rangle &= \left\langle x \left(\frac{2\pi ny}{d} \right) \right\rangle \\ \langle sx_m \rangle &= \left\langle sx \left(\frac{2\pi my}{d'} \right) \right\rangle, \end{aligned} \quad (20)$$

where

$$\langle \dots \rangle = \text{Tr}_{(X)} [P(X) \dots] = S \sum_{s=\pm 1} \frac{1}{L} \int_0^{Md=M'd'=L} dy P(s, y) \dots \quad (21)$$

with $x_\alpha \equiv \{c, s\}$ and, correspondingly, $x(\dots) \equiv \{\cos(\dots), \sin(\dots)\}$. With definitions (20) we can finally rewrite the distribution function in the symmetry adapted form. It reads

$$\begin{aligned} P(s, y) &= \frac{1}{2S} + \frac{1}{S} \sum_{n=1}^{\infty} \left[\langle c_n \rangle \cos\left(\frac{2\pi ny}{d}\right) + \langle s_n \rangle \sin\left(\frac{2\pi ny}{d}\right) \right] \\ &+ \frac{1}{2S} \langle s \rangle s + \frac{1}{S} \sum_{m=1}^{\infty} \left[\langle sc_m \rangle s \cos\left(\frac{2\pi my}{d'}\right) + \langle ss_m \rangle s \sin\left(\frac{2\pi my}{d'}\right) \right]. \end{aligned} \quad (22)$$

Substituting the expansion (22) back into the effective excluded volume (13) and assuming

L to be large, we can reduce $H_{eff}(X_1)$ to a simpler form. It is given by

$$H_{eff}(X_1) = \bar{\rho}S \sum_{s_2=\pm 1} \int_0^L dy_2 \lambda(y_{12}, s_1 s_2) P(s_2, y_2), \quad (23)$$

where

$$\lambda(y_{12}, s_1 s_2) = \int_0^L \Theta [\xi(x_{12}, y_{12}, s_1 s_2) - r_{12}] dx_2 = \lambda_0(y_{12}) + s_1 s_2 \lambda_1(y_{12}) \quad (24)$$

plays the role of an excluded interval for fixed relative positions and orientations of two molecules.

This excluded area depends only on the relative orientation between the molecules and on their relative distance. There are two cases: with particles pointing in the same direction ($s_1 s_2 = 1$), or in the opposite direction ($s_1 s_2 = -1$). The exemplary cases are shown in Fig. (4). For our molecules the excluded area is calculated analytically, but only for the needle-like bananas the formulas can be cast in a concise form. For $s_1 s_2 = 1$ they read

$$\left\{ \begin{array}{ll} -\frac{y_{12}+2l \sin \psi}{\tan \psi} \leq x_{12} \leq \frac{y_{12}+2l \sin \psi}{\tan \psi} & -2l \sin \psi \leq y_{12} \leq -l \sin \psi \\ \frac{y_{12}}{\tan \psi} \leq x_{12} \leq -\frac{y_{12}}{\tan \psi} & -l \sin \psi \leq y_{12} \leq 0 \\ -\frac{y_{12}}{\tan \psi} \leq x_{12} \leq \frac{y_{12}}{\tan \psi} & 0 \leq y_{12} \leq l \sin \psi \\ \frac{y_{12}-2l \sin \psi}{\tan \psi} \leq x_{12} \leq \frac{-y_{12}+2l \sin \psi}{\tan \psi} & l \sin \psi \leq y_{12} \leq 2l \sin \psi \end{array} \right. \quad (25)$$

and for $s_1 s_2 = -1$

$$\left\{ \begin{array}{ll} x_{12} = -\frac{y_{12}}{\tan \psi} & -2l \sin \psi \leq y_{12} \leq -l \sin \psi \\ -\frac{y_{12}}{\tan \psi} \leq x_{12} \leq \frac{y_{12}+2l \sin \psi}{\tan \psi} & -l \sin \psi \leq y_{12} \leq 0 \\ \frac{y_{12}}{\tan \psi} \leq x_{12} \leq \frac{-y_{12}+2l \sin \psi}{\tan \psi} & 0 \leq y_{12} \leq l \sin \psi \\ x_{12} \leq \frac{y_{12}}{\tan \psi} & l \sin \psi \leq y_{12} \leq 2l \sin \psi. \end{array} \right. \quad (26)$$

For needle-like boomerangs λ s take particularly simple form. They read

$$\lambda_0(y_{12}) = \left\{ \begin{array}{ll} l \cos \psi & |y_{12}| < l \sin \psi \\ \frac{-|y_{12}|+2l \sin \psi}{\tan \psi} & l \sin \psi \leq |y_{12}| \leq 2l \sin \psi, \end{array} \right. \quad (27)$$

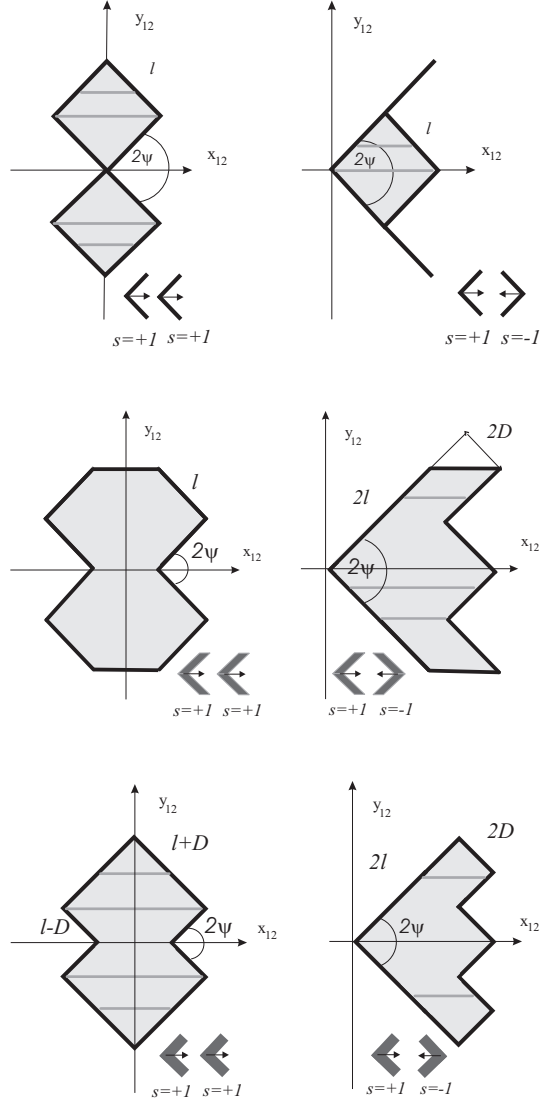


FIG. 4: Excluded area in (x_{12}, y_{12}) plane for needle-like, HB and SB particles with $2\psi = \pi/2$ and $\delta = 1/3$.

$$\lambda_1(y_{12}) = \begin{cases} \frac{2|y_{12}| - l \sin \psi}{\tan \psi} & |y_{12}| < l \sin \psi \\ \frac{-|y_{12}| + 2l \sin \psi}{\tan \psi} & l \sin \psi \leq |y_{12}| \leq 2l \sin \psi. \end{cases} \quad (28)$$

Examples of λ_s for needle-like boomerangs, HB and SB molecules are shown in Fig. (5).

The next step is to perform the integration in (23) by replacing y_{12} with y , where $y_2 =$

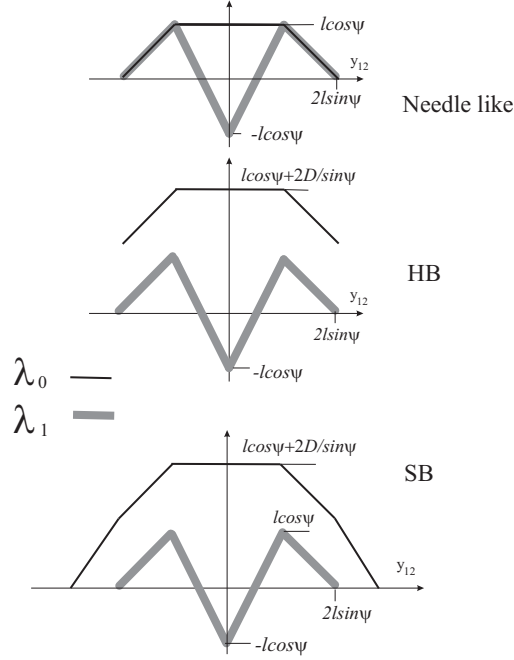


FIG. 5: λ functions for needle-like boomerangs, HB and SB molecules. Coordinates of characteristic points of the functions are also given.

$y_1 + y$. In the limit of large L the final formula for the effective excluded volume is given by

$$\begin{aligned}
l^2 \sin(2\psi) H_{eff}(s_1, y_1) = & \rho A_0 + \rho B_0 \langle s \rangle s_1 + \\
& 2\rho \sum_{n=1}^{\infty} \left\{ \langle c_n \rangle \left[A_n \cos\left(\frac{2\pi n y_1}{d}\right) - C_n \sin\left(\frac{2\pi n y_1}{d}\right) \right] + \right. \\
& \left. \langle s_n \rangle \left[A_n \sin\left(\frac{2\pi n y_1}{d}\right) + C_n \cos\left(\frac{2\pi n y_1}{d}\right) \right] \right\} + \\
& 2\rho s_1 \sum_{m=1}^{\infty} \left\{ \langle s c_m \rangle \left[B_m \cos\left(\frac{2\pi m y_1}{d'}\right) - D_m \sin\left(\frac{2\pi m y_1}{d'}\right) \right] + \right. \\
& \left. \langle s s_m \rangle \left[B_m \sin\left(\frac{2\pi m y_1}{d'}\right) + D_m \cos\left(\frac{2\pi m y_1}{d'}\right) \right] \right\}, \quad (29)
\end{aligned}$$

where the coefficients of the expansion are defined as

$$A_n = l^2 \sin(2\psi) \alpha(\psi, \delta, k_n) = \int_{-2l \sin \psi}^{2l \sin \psi} \lambda_0(y) \cos\left(\frac{2\pi n y}{d}\right) dy, \quad (30)$$

$$B_m = l^2 \sin(2\psi) \beta(\psi, \delta, k'_m) = \int_{-2l \sin \psi}^{2l \sin \psi} \lambda_1(y) \cos\left(\frac{2\pi m y}{d'}\right) dy, \quad (31)$$

$$C_n = l^2 \sin(2\psi) \gamma(\psi, \delta, k_n) = \int_{-2l \sin \psi}^{2l \sin \psi} \lambda_0(y) \sin\left(\frac{2\pi n y}{d}\right) dy, \quad (32)$$

$$D_m = l^2 \sin(2\psi) \sigma(\psi, \delta, k'_m) = \int_{-2l \sin \psi}^{2l \sin \psi} \lambda_1(y) \sin\left(\frac{2\pi m y}{d'}\right) dy. \quad (33)$$

Here ρ is defined in Eq.(1) and k, k' are dimensionless wave vectors given by $k = \frac{\pi l \sin \psi}{d}$ and $k' = \frac{\pi l \sin \psi}{d'}$, respectively. As a result of the condition that $L = Md = M'd'$ we additionally have a limitation $Mk' = M'k$ imposed on wave vectors. Substitution of $n = m = 0$ in (30) and (31) gives A_0 and B_0 .

Formally, the coefficients (30-33) are the Fourier transforms of λ_α , Eq.(24). For the case of needle-like bananas these coefficients are of particularly simple form, namely

$$\begin{aligned} \alpha(\psi, \delta, 0) &= \frac{3}{2}, \quad \beta(\psi, \delta, 0) = \frac{1}{2}, \quad \gamma(\psi, \delta, k) = \sigma(\psi, \delta, k) = 0, \\ \alpha(\psi, \delta, k) &= \frac{[2 \cos(2k) + 1] \sin^2(k)}{2k^2}, \\ \beta(\psi, \delta, k) &= \frac{[2 \cos(2k) - 1] \sin^2(k)}{2k^2}, \end{aligned} \quad (34)$$

where $k = \frac{l\pi \sin \psi}{d}$. They are shown in Fig. (6).

Taking definitions (20) the nonlinear integral equation (15) becomes reduced to an infinite set of nonlinear algebraic equations for the order parameters

$$\begin{pmatrix} \langle x_n \rangle \\ \langle s x_m \rangle \\ \langle s \rangle \end{pmatrix} = Z^{-1} T_{(X_1)} \left[\begin{pmatrix} x \left(\frac{2\pi n y_1}{d} \right) \\ s_1 x \left(\frac{2\pi m y_1}{d'} \right) \\ s_1 \end{pmatrix} \exp(-H_{eff}) \right]. \quad (35)$$

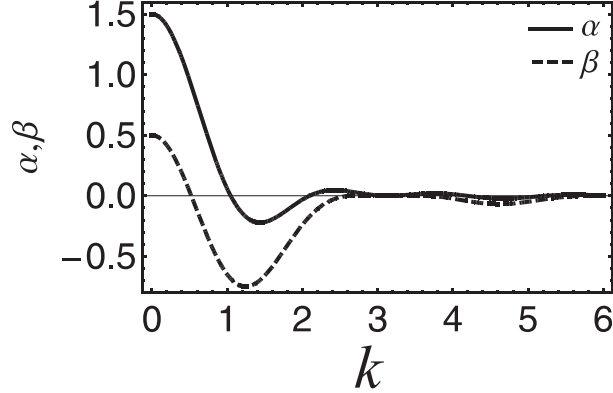


FIG. 6: The k -dependence of the coefficients α and β for needle-like boomerangs.

The corresponding stationary excess free energy in the limit of large L is given by

$$\begin{aligned}
\frac{f[P_s]}{l^2 \sin(2\psi)} &= \bar{\rho} \langle \ln P_s \rangle + \frac{\bar{\rho}}{2} \langle H_{eff} \rangle = -\frac{\bar{\rho}}{2} \langle H_{eff} \rangle - \bar{\rho} \ln Z \\
&= -\frac{\bar{\rho}^2}{2} \left[A_0 + B_0 \langle s \rangle^2 + 2 \sum_{n=1}^{\infty} A_n (\langle c_n \rangle^2 + \langle s_n \rangle^2) \right. \\
&\quad \left. + 2s_1 \sum_{m=1}^{\infty} B_m (\langle sc_m \rangle^2 + \langle ss_m \rangle^2) \right] - \bar{\rho} \ln Z. \tag{36}
\end{aligned}$$

The Eqs (36) should be solved for given d, d' and appropriately chosen M, M' . Then the equilibrium structure is identified with the absolute minimum of (36) taken with respect to the stationary solutions and with respect to the periodicities d, d' . Note that the trivial nematic state corresponding to $\langle s \rangle = \langle c_n \rangle = \langle s_n \rangle = \langle sc_n \rangle = \langle ss_n \rangle = 0$ ($\forall n$) always satisfies Eqs (35). Problem that remains is to identify all nontrivial solutions of Eqs (35), where at least one of the order parameters becomes nonzero. A systematic way of finding these solutions is bifurcation analysis [35]. Here, we apply this technique to analyze bifurcation from the nematic phase. We also determine exemplary phase diagrams from the full minimization of the free energy in different phases, in a wide range η .

C. Bifurcation analysis

Now we consider a bifurcation from a perfectly aligned nematic phase. Close to the bifurcation point the difference between the states is arbitrarily small for each d, d' , which enables one to linearize the RHS of Eqs (35) with respect to the order parameters. The analysis is carried out by taking the needle-like boomerangs as reference. The results are

$$\begin{pmatrix} \langle c_n \rangle \\ \langle s_n \rangle \end{pmatrix} = -\rho \mathbf{A}_n \begin{pmatrix} \langle c_n \rangle \\ \langle s_n \rangle \end{pmatrix}, \quad (37)$$

$$\begin{pmatrix} \langle sc_m \rangle \\ \langle ss_m \rangle \end{pmatrix} = -\rho \mathbf{B}_m \begin{pmatrix} \langle sc_m \rangle \\ \langle ss_m \rangle \end{pmatrix}, \quad (38)$$

$$\langle s \rangle = \rho \beta(0) \langle s \rangle, \quad (39)$$

where 2 by 2 arrays $\mathbf{A}_n, \mathbf{B}_m$ are given by

$$\mathbf{A}_n = \begin{pmatrix} \alpha(\psi, \delta, k_n) & \gamma(\psi, \delta, k_n) \\ -\gamma(\psi, \delta, k_n) & \alpha(\psi, \delta, k_n) \end{pmatrix} \quad (40)$$

and

$$\mathbf{B}_m = \begin{pmatrix} \beta(\psi, \delta, k'_m) & \sigma(\psi, \delta, k'_m) \\ -\sigma(\psi, \delta, k'_m) & \beta(\psi, \delta, k'_m) \end{pmatrix}. \quad (41)$$

The homogeneous equations (37-39) have a nontrivial solution given that at least one of the equations

$$\det(\mathbf{1} + \rho \mathbf{A}_n) = 0, \quad (42)$$

$$\det(\mathbf{1} + \rho \mathbf{B}_m) = 0, \quad (43)$$

$$\rho \equiv \rho_0 = -\frac{1}{\beta(0)} \quad (44)$$

is satisfied for a positive ρ . By solving (42,43) for ρ we obtain two functions: $\rho(k_n)$ and $\rho'(k'_m)$, respectively, together with ρ_0 . The bifurcation density is then identified with the lowest positive value taken out of

$$\left\{ \text{Min}_{\{k_n\}} [\rho(k_n)], \text{Min}_{\{k'_m\}} [\rho'(k'_m)], \rho_0 \right\}. \quad (45)$$

For majority of cases studied we will assume the director to be perpendicular both to the layer normal and the molecule's dipole moment, Fig.(2). In this case $\lambda = \lambda(|y_{12}|, s_1 s_2)$ in Eq. (24). Consequently, we can choose ϕs in (19) to vanish and consider the case of vanishing $\langle s_n \rangle$ and $\langle s s_m \rangle$. The corresponding bifurcation density is then the lowest positive value out of

$$\left\{ \text{Min}_{\{k_n\}} \left[\frac{-1}{\alpha(k_n)} \right], \text{Min}_{\{k'_m\}} \left[\frac{-1}{\beta(k'_m)} \right], \frac{-1}{\beta(0)} \right\}. \quad (46)$$

As an example we start with the discussion of bifurcation for needle-like boomerangs. It turns out that the most stable structure bifurcating from the nematic phase is the antiferroelectric smectic A phase (AF). To see this consider the behavior of $\alpha(k_n)$ and $\beta(k'_m)$, shown in Fig. (6). One observes that β attains the absolute minimum for $k'_{0,m} = 1.246$ and α for $k_{0,n} = 1.438$, and that these points correspond to the layer thicknesses of $d'_{0,m} = \frac{lm\pi \sin \psi}{k'_{0,m}} = 2.52ml \sin \psi$ and $d_{0,n} = \frac{ln\pi \sin \psi}{k_{0,n}} = 2.184nl \sin \psi$, respectively. Consequently, the physical bifurcation to the smectic A phase should occur for $n = 1$ with $d_0 \approx 2.18l \sin(\psi) = 1.09(2l \sin(\psi))$ and bifurcation to the smectic AF phase for $m = 1$ with $d_0 \approx 2.51 \sin(\psi) = 1.26(2l \sin(\psi))$. Since the minimum of B_m is deeper, the expected lamellar phase bifurcating from the nematic phase will be of the antiferroelectric type. The value of this minimum determines the bifurcation density ($\rho_{bif} = -\frac{1}{B^{\min}}$). Then, the distribution function at the bifurcation point will take the form

$$P(s, y) = \frac{1}{2S} + \frac{1}{S} \langle s c_1 \rangle s \cos \left(\frac{2\pi y}{2.52l \sin \psi} \right) + \dots \quad (47)$$

IV. POSSIBLE STRUCTURES

In general, possible two-dimensional structures that can be expected in boomerang systems are given in Fig.(7). The low density phase, the nematic phase, can be here of two types: a standard nematic phase in which the same (on average) number of boomerangs is pointing to the right as to the left. When one type of the orientation prevails then one deals with the polar nematic (or ferroelectric nematic). Upon an increase of density a transition to smectic phase, which is characterized by a regular modulation of the density profile due to presence of the layers, may occur. Three different smectic phases are plausible: typical smectic A phase, where left and right-pointing particles are equinumbered (on average), ferroelectric smectic A phase when the particles oriented in one direction overwhelm the

number of the oppositely oriented particles, and smectic AF phase, in which the particles in subsequent layers have opposite orientations. Note that the period d' of the layers with particles with the same average orientation in the antiferroelectric phase is twice the smectic period d ($M = 2M' = 2$), whereas in the polar phase they attain the same value. The occurrence of such phases will depend on the structure of the particles themselves as well as on the density.

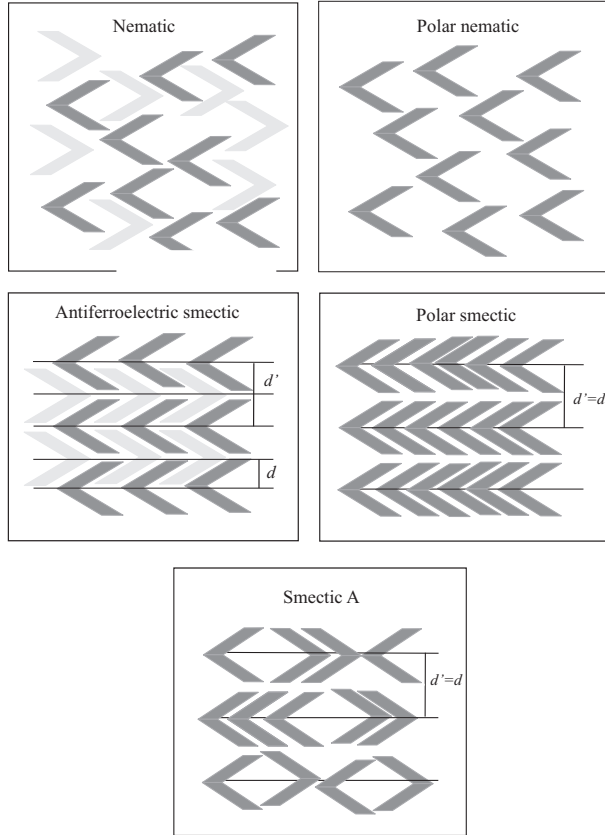


FIG. 7: Possible arrangements of perfectly aligned bent-core molecules. For better visibility the molecules pointing in opposite direction are drawn in different shades of gray.

V. BOOMERANGS OF ARMS WITH FINITE WIDTH

A. The HB molecules

The model of the needle-like boomerangs can be extended to the case when arms are of finite width in many different ways of which we choose HB and SB shapes. The HB case is

given in Fig.(1b). For HB molecules the coefficients α and β are given by

$$\begin{aligned}\alpha(\psi, \delta, k) &= \frac{[1 + 2 \cos(2k)] \sin^2 k + \frac{4\delta}{\sin(2\psi)} k \sin(4k)}{2k^2}, \\ \beta(\psi, \delta, k) &= \frac{[-1 + 2 \cos(2k)] \sin^2 k}{2k^2}, \\ \alpha(\psi, \delta, k \rightarrow 0) &= \frac{3}{2} + \frac{8\delta}{\sin(2\psi)}, \\ \beta(\psi, \delta, k \rightarrow 0) &= \frac{1}{2}.\end{aligned}\tag{48}$$

Note that the coefficient β is here exactly the same as in the case of the needle-like

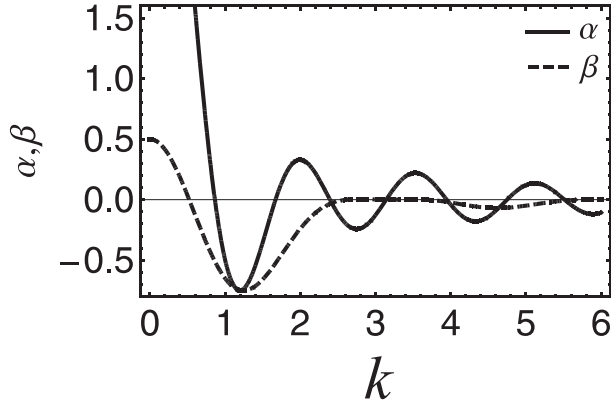


FIG. 8: The Fourier transforms α and β for the condition $\delta = 0.3654 \sin(2\psi)$.

boomerangs. It turns out, however, that when the condition $\delta = 0.3654 \sin(2\psi)$ is fulfilled, the minimum of α and the minimum of β attain the same value $\beta_{min} = \alpha_{min} = -0.749956$ (see Fig.(8)). This condition provides a set of values for the parameters serving as a limiting case when the bifurcation from the nematic phase to ordinary smectic A becomes observed.

Using the density of the form $\rho = \eta \frac{\sin 2\psi}{2\delta}$ one can now obtain the bifurcation diagram as given in Fig.(9). Similarly as in [25] the most common smectic phase obtained here is the antiferroelectric smectic A given by the blue region. It is possible, however, to obtain different kind of solutions - the red region in Fig. (9) corresponds to the cases where the set of the angle-arm thickness promotes the typical smectic A order. The lines provide condition where the assumed packing fraction η is equal to 0.1, 0.5 and 0.9. These packing fraction limits do not, however, rule out the occurrence of the other than antiferroelectric

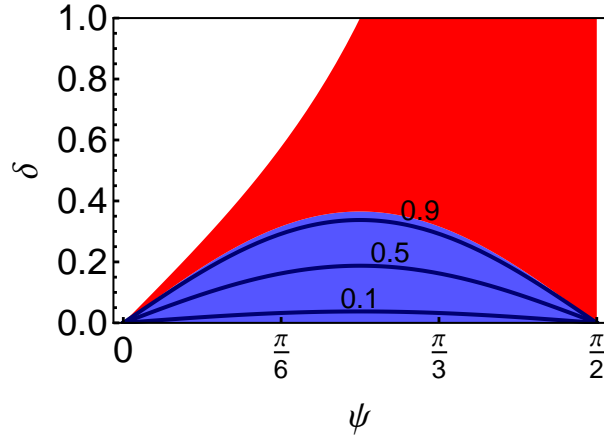


FIG. 9: (Color online) Bifurcation diagram for HB boomerangs. The blue region corresponds to the cases where nematic-antiferroelectric smectic A bifurcation takes place and the red region corresponds to the cases where the nematic-smectic A bifurcation undergoes. The black lines are the density limits with the packing fraction η given in the legend.

smectic phases, which may occur as the result of the phase transition between two different types of smectics. Such an information can be obtained by solving numerically the self consistency equations for each set of molecular parameters and comparing the free energies of the solutions.

B. The SB molecules

In the case of the SB molecules the calculation of the Fourier transforms for the excluded slice becomes more complicated. One must consider here three cases with different antiparallel arrangements of the molecules as shown in Fig.(10). The first two appear when the

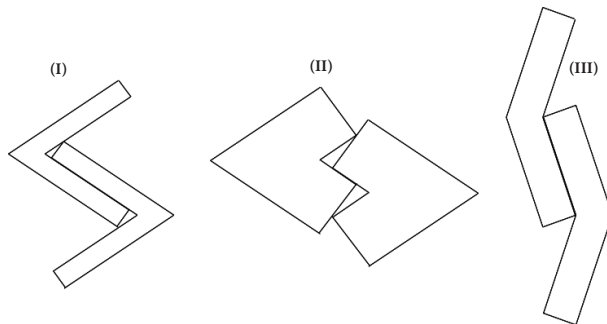


FIG. 10: Three cases of antiparallel arrangements for SB molecules.

opening angle 2ψ is smaller than $\pi/2$. The first case occurs also when arms are thin, namely their width is smaller than $1/[\cot(\psi) + \csc(2\psi)]$. The corresponding normalized α and β functions for the cases (I)-(III) are given in Appendix A. It turns out that the theoretical spectrum of stable phases is now much richer. Examining the position of relative minima for α and β (see Fig.(11)) one observes bifurcations to different phases. More specifically,

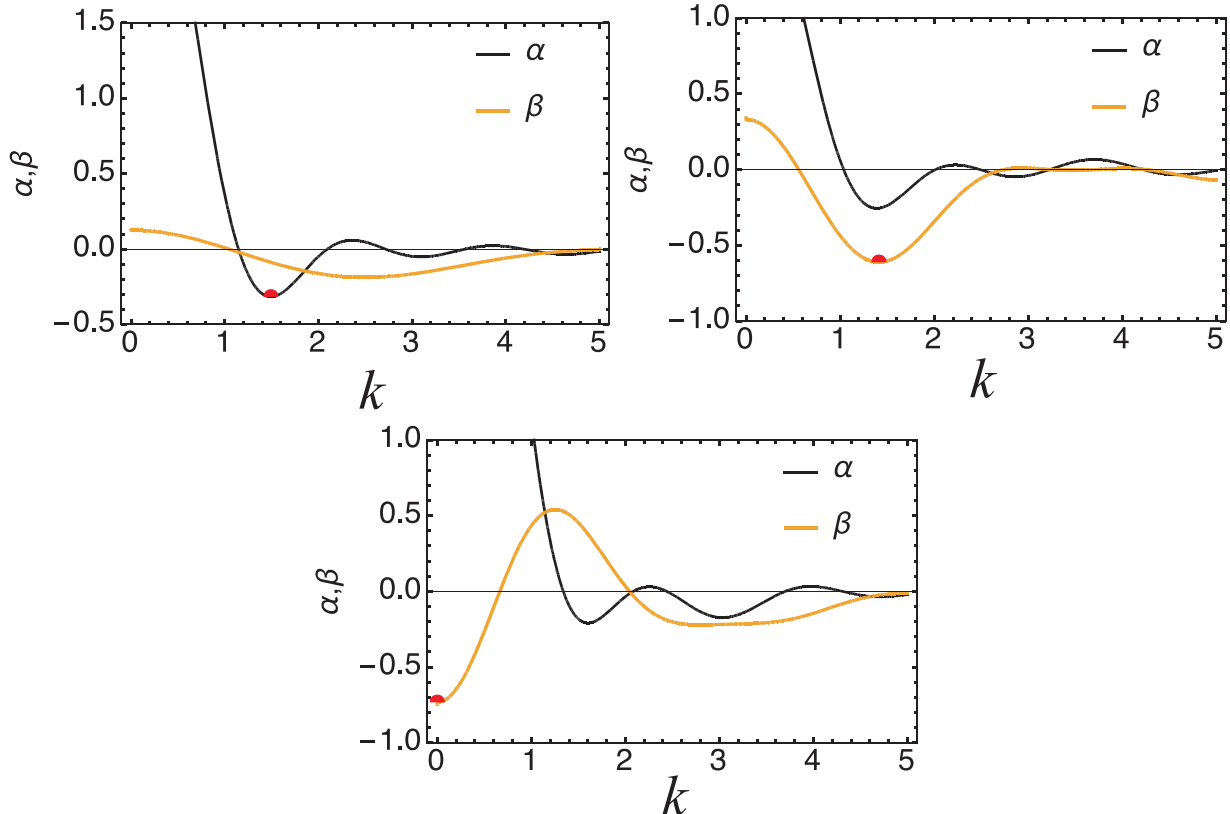


FIG. 11: (Color online) Different relations between absolute minimum of α and β . Left top diagram corresponds to $\psi = \pi/4$ and $\delta = 0.5$ and bifurcation to smectic A phase. Right top diagram corresponds to $\psi = \pi/4$ and $\delta = 0.1$, where bifurcation is to antiferroelectric phase. The bottom diagram corresponds to $\psi = \pi/3$ and $\delta = 1.0$ and bifurcation to ferroelectric nematic phase.

the first panel of (11) illustrates the case where the bifurcation to the smectic A phase takes place, which is connected with the coefficient α having a deeper global minimum than β and of negative value. The next panel shows the case when the minimum of β is deeper than that of α , hence the bifurcating phase will be of the antiferroelectric type. When the minima (negative) are about the same depth we may also expect an incommensurate smectic phase to become absolutely stable. Within our formalism this case can be studied by taking a commensurate approximation, where both minima are approximated by appropriate choice

of k, k' and M, M' .

In the case of SB molecules one also observes another interesting type of the bifurcation scenario. In the third panel the profile of β shows absolute minimum for $k_m = 0$. Such a behavior is symptomatic for the polar nematic phase, which has not been reported previously. The complete bifurcation diagram is presented in Fig.(12). The blue region in this diagram

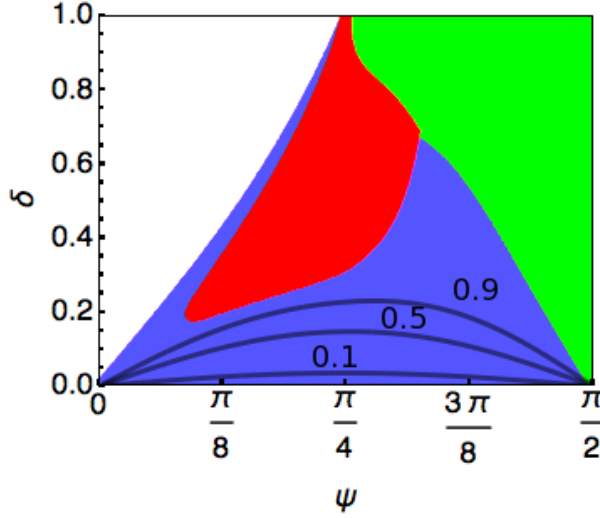


FIG. 12: (Color online) Bifurcation diagram for SB boomerangs. The blue region corresponds to the cases where nematic-antiferroelectric bifurcation takes place. The red one is responsible for nematic-smectic A order. The green area corresponds to the nematic - polar nematic bifurcation. The black lines are the density limits, where packing fraction η is given in the legend.

corresponds to the apex angle and arm thickness values where the bifurcation from the nematic to the antiferroelectric phase takes place. The red area corresponds to the nematic-smectic A bifurcations and in the green area the bifurcation is dominated by the polar nematic phase. The black lines are the guide lines at which the packing fractions are given as in the legend. We have also checked a few cases for a possibility to get stable incommensurate smectics of A type and smectic C phases, where the steric dipole is not perpendicular to the director, but found no one stable.

C. Exemplary results of full minimization

Here the free energy of different smectic and polar nematic phases is calculated for exemplary molecular shapes to identify the stable phases as function of packing fraction. It turns out that for majority of cases the calculations involving terms up to $n = m = 4$ in (28)

and (34) give excellent quantitative predictions for the equilibrium structures. The obtained results are consistent with the phase diagram maps, Figs (9, 12), in apex angle- arm's width plane.

We start with the case of stable smectic AF phase, represented by the blue region in Figs (9,12). Figs (13, 14) compare the equilibrium values of leading order parameters for this structure as function of packing fraction and arm's width for $\psi = \pi/3$. It turns out

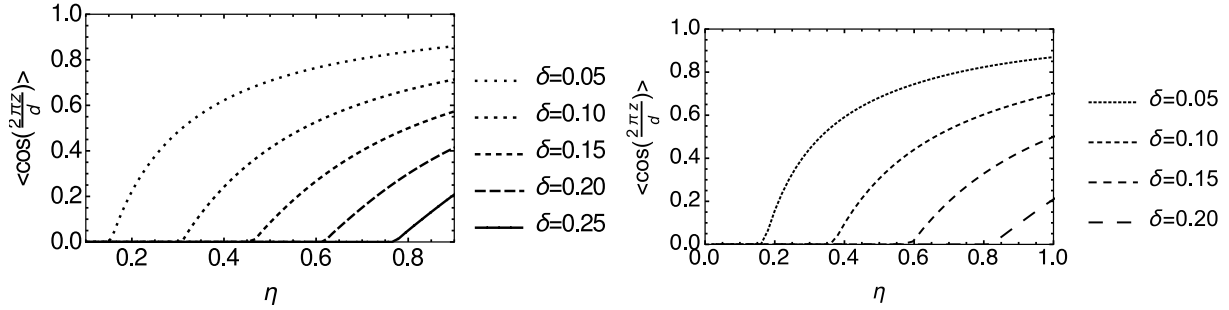


FIG. 13: Typical behaviour of equilibrium order parameter $\langle c \rangle$ for the cases with stable smectic AF phase, obtained for different packing fractions η and the apex angle $2\psi = 2\pi/3$. The panel on the left is for the HB molecules while the panel on the right is for the SB molecules.

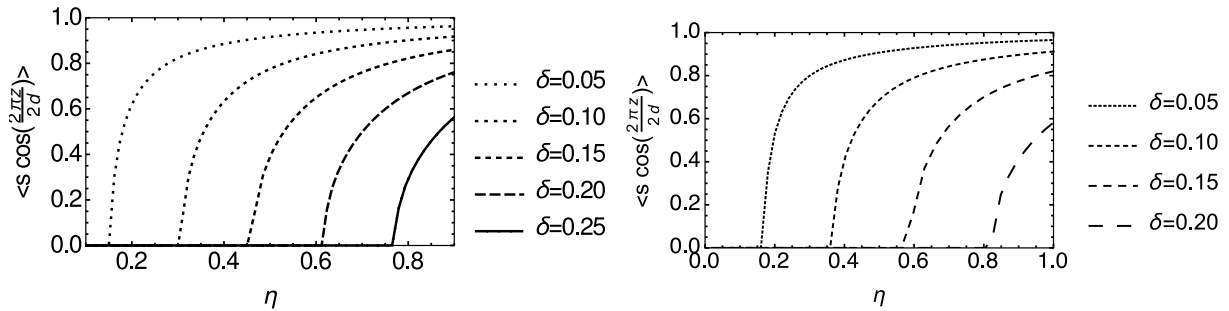


FIG. 14: Typical behaviour of equilibrium order parameter $\langle sc \rangle$ for the cases with stable smectic AF phase, obtained for different packing fractions η and the apex angle $2\psi = 2\pi/3$. The panel on the left is for the HB molecules while the panel on the right is for the SB molecules.

that the change of the arm endings strongly influences the behavior of the order parameters, especially when the thickness of the arms increases. As expected, for thin arms, where for

instance $\delta = 0.05$, the profiles of the order parameters (and the bifurcation points) are very similar. For larger values of δ the bifurcation point for the SB boomerangs shifts toward higher packing fractions. For $\delta = 0.25$ one does not observe the stable smectic AF phase whereas for the HB boomerangs this value is still attainable.

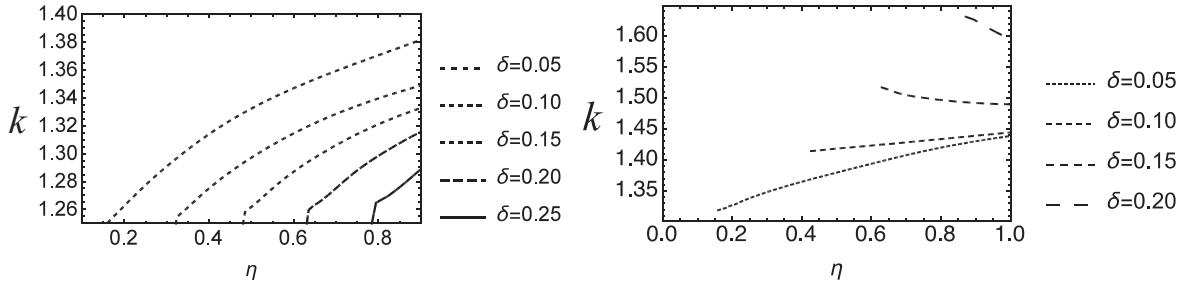


FIG. 15: Equilibrium wave vector k ($k' = k/2$) in stable smectic AF phase obtained for different packing fractions and the apex angle $2\psi = 2\pi/3$ for the HB molecules (left) and for the SB molecules (right). The layer thickness is proportional to inverse of k .

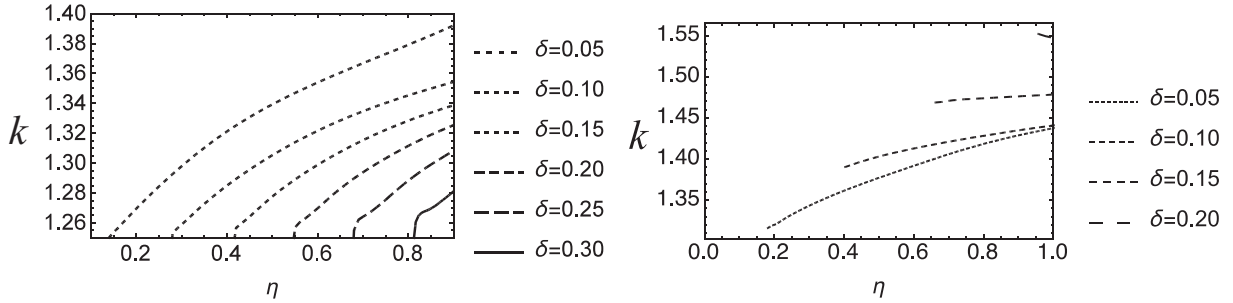


FIG. 16: Equilibrium wave vector k ($k' = k/2$) in stable smectic AF phase obtained for different packing fractions and the apex angle of $2\psi = 2\pi/4$ for the HB molecules (left) and for the SB molecules (right). The layer thickness is proportional to inverse of k .

In Figs (15) and (16) the equilibrium wave vector k of the smectic AF phase, obtained for different packing fractions η and the apex angle of $2\psi = 2\pi/3$ and $2\psi = 2\pi/4$, respectively, is presented for HB and SB molecules. In case of HB molecules the k vector increases with the packing fraction, which means diminishing of the layer thickness. For the SB molecules the wave vector k can show different behaviour. In the case of $2\psi = 2\pi/3$, for thicker

arms ($\delta > 0.15$), the wave vector diminishes with the packing fraction and hence the layer thickness increases.

The results showing stable smectic A, polar nematic and ferroelectric smectic A phases are shown in Figs (17-19). Note that structures became stable at high molecular packing fractions η_{mol} .

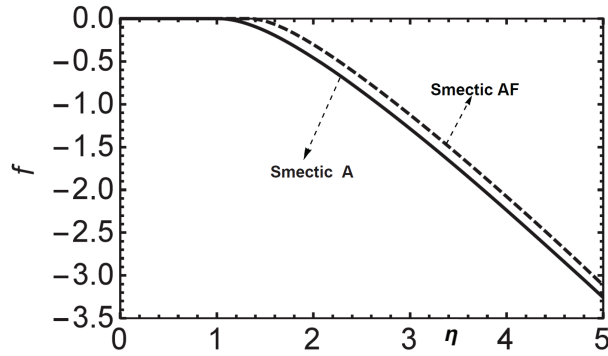


FIG. 17: Free energies vs packing fraction η for two competing structures: smectic A and smectic AF of HB system. Molecular parameters are $\delta = 0.5$ and $\psi = \frac{\pi}{4}$. The structure of lower free energy is smectic A. Note that according to (17) smectic A becomes stable for $\eta_{mol} > 0.55$ ($\eta > 1$).

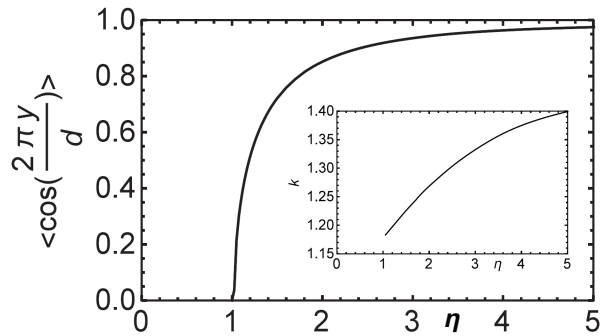


FIG. 18: Equilibrium, leading order parameter for stable smectic A phase of HB system. Equilibrium wave vector k is shown as inset. Molecular parameters are $\delta = 0.5$ and $\psi = \frac{\pi}{4}$.

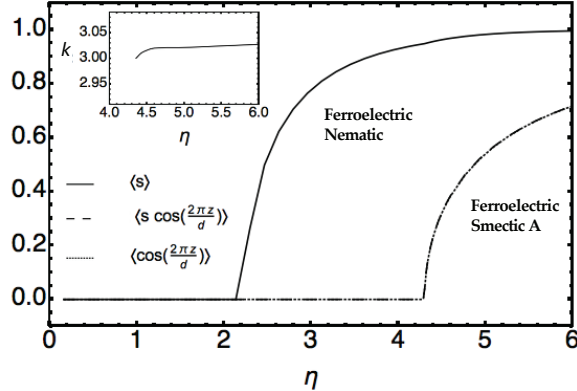


FIG. 19: Leading equilibrium order parameters for stable ferroelectric nematic and ferroelectric smectic A phases of SB molecules, obtained for different packing fractions. Molecular parameters are $\delta = 1$ and $\psi = \frac{\pi}{3}$. The wave vector k ($k' = k/2$) in ferroelectric smectic A phase is shown as inset. The layer thickness is proportional to inverse of k . Note that taking PL rescaling (17) the ferroelectric nematic becomes stable for $\eta_{mol} > 0.74$ ($\eta > 2.1$).

VI. SUMMARY AND CONCLUSIONS

We have studied two-dimensional ensembles of bent-core shaped molecules of zero and finite arm width, confined to the planar surface. Using second virial Onsager density functional theory and the bifurcation analysis the role of excluded volume interactions in stabilizing different structures and its influence on local polarization have been examined.

Onsager's theory reconstructs main conclusions from [25] about occurrence of the antiferroelectric smectic A phase and proves that AF smectic order is indeed robust for 2D bent-core system. It also stays in line with experimental observations of Gong and Wan for banana-shaped P-n-PIMB molecules absorbed onto a HOPG surface [1]. This is in spite of the fact that we disregarded any orientationally dependent interaction between substrate and molecules ($V_{ext} = 0$ in Eq. (5)), limiting the role of the surface to confine molecules in 2D (assumption of strong planar anchoring). That the surface can be considered smooth at the lengthscale of the molecular size is justified by comparing the size of bent-core P-n-PIMB molecules (a few nanometers) and the lattice spacing of HOPG (0.25nm). Also we should add that our dimensionless shape parameter δ corresponds to $\delta \lesssim 0.2$ for P-n-PIMB.

We find neither smectic C nor incommensurate smectic order to become likely for these systems. However, the possibility to obtain ferroelectric smectic A and ferroelectric nematic

molecular order are foreseen from Onsager's theory. We show that the actual state of the lamellar structures depend strictly on the behavior of the Fourier transforms of the appropriately recognized parts of the excluded volume. According to this behavior different transitions are plausible, yet other phases than antiferroelectric smectic A can be realized for large packing fraction η_{mol} .

We show that small structural modifications like the change of the arm edges, the apex angle, or thickness of the arm may substantially influence the the behavior of the order parameters, wave vector and even phase diagrams. For the case of HB molecules only antiferroelectric smectic A and smectic A are possible, whereas for the SB molecules ferroelectric order can also occur.

We also demonstrate that the width of the molecule arm influences the layer thickness.

The new phases found (ferroelectric, ordinary smectic A) are expected to appear at higher packing fractions η_{mol} , Figs. (17-19). Since $\eta > 1$, this rises an issue as whether such phases should not be excluded on the ground that Onsager's DFT is formally justified in the dilute gas limit (DGL). The reason we believe that this is not the case is that the mathematically similar form of the free energy as that of Onsager's, Eqs. (12,13), can be obtained with a more elaborated approach and without referring to DGL. Examples are Parsons-Lee scaling (PLS) [30–32], or y -expansion. The difference between the resulting free energies and Eq.(12) is that the quadratic coefficient in reduced density/packing fraction that appears there is replaced by a more complicated, rational function in these parameters, Eq. (17).

Finally, we should mention that we carried out our calculations by assuming that the reference nematic system is perfectly aligned and the director is uniform in 2D. An interesting alternative for the director would be to assume that it forms periodic splay-bend-like structures [33, 34]. Indeed, simulations of González *et al.* [25], indicate that such splay-bend instabilities are likely to exist in a two-dimensional system of hard, banana-shaped needles, but they did not observe any long-range splay-bend nematic order. A question whether such splay-bend structures can be stabilized in 2D prior to any smectic ordering is more challenging to answer, especially in simulations [22], and will be addressed in our forthcoming publication.

VII. APPENDIX A

We add here, for completeness, the formulas for the Fourier transforms of the interaction-excluded slice kernel for the SB boomerangs discussed in Section V. Subscripts refer to coefficients calculated for cases shown in Fig. (10).

$$\begin{aligned} \alpha_I(\psi, \delta, k) = & \frac{1}{8k^2} [4 \sec^2(\psi) \cos(2k(\delta \cot(\psi) - 1)) \cos^2(k - \delta k \cot(\psi)) + \\ & + \cos(2\psi) \sec^2(\psi) \cos(2\delta k \cot(\psi)) - 2 \cos(k(\delta \csc(\psi) \sec(\psi) - 2)) + \\ & + 2 \cos(2k) \cos(2\psi) \sec^2(\psi) - \cos(4k) (\sec^2(\psi) + 2) - 2] \end{aligned} \quad (49)$$

$$\begin{aligned} \alpha_{II}(\psi, \delta, k) = & \frac{1}{8k^2} \{ -\tan(\psi) \csc(2\psi) [2 \cos(4k \cos^2(\psi)(\delta \cot(\psi) - 1)) - \\ & - 4 \cos(2k(\delta \cot(\psi) - 1)) - 2 \cos(4k(\delta \cot(\psi) - 1)) + \cos(4k - 2\psi) \\ & - 2 \cos(2(k - \psi)) - 2 \cos(2(k + \psi)) + \cos(2(2k + \psi)) + 4 \cos(4k) + 2 \cos(2\psi)] \} \end{aligned} \quad (50)$$

$$\begin{aligned} \alpha_{III}(\psi, \delta, k) = & \frac{1}{8k^2} [4 \sec^2(\psi)(\cos(2k(\delta \cot(\psi) - 1)) + \cos(2k) + 1) \sin(\delta k \cot(\psi)) \\ & \cdot \sin(k(2 - \delta \cot(\psi))) - 2(\cos(2k(\delta \cot(\psi) - 1)) - 2 \cos(2k) + \cos(4k))] \end{aligned} \quad (51)$$

$$\begin{aligned} \beta_I(\psi, \delta, k) = & \frac{1}{8k^2} [(\sec^2(\psi) - 2) \cos(2\delta k \cot(\psi)) + 2(\cos(k(2 - \delta \csc(\psi) \sec(\psi))) + \\ & + \sec^2(\psi) (2 \cos(2k(\delta \cot(\psi) - 1)) \sin^2(k - \delta k \cot(\psi)) + \cos(2k) \cos(2\psi)) - 1) + \\ & + \cos(4k) (\sec^2(\psi) - 2)] \end{aligned} \quad (52)$$

$$\begin{aligned} \beta_{II}(\psi, \delta, k) = & -\frac{1}{16k^2} [\sec^2(\psi) (-2 \cos(4k \cos^2(\psi)(\delta \cot(\psi) - 1)) - 4 \cos(2k(\delta \cot(\psi) - 1)) + \\ & + 2 \cos(4k(\delta \cot(\psi) - 1)) + \cos(4k - 2\psi) - 2 \cos(2(k - \psi)) - \\ & - 2 \cos(2(k + \psi)) + \cos(2(2k + \psi)) + 2 \cos(2\psi) + 4] \end{aligned} \quad (53)$$

$$\begin{aligned} \beta_{III}(\psi, \delta, k) = & \frac{1}{8k^2} [-\sec^2(\psi) \cos(4k(\delta \cot(\psi) - 1)) + 2(\sec^2(\psi) + 1) \cos(2k(\delta \cot(\psi) - 1)) + \\ & + 2 \cos(2k) \cos(2\psi) \sec^2(\psi) + \cos(4k) (\sec^2(\psi) - 2) - 4] \end{aligned} \quad (54)$$

$$\beta_{0I}(\psi, \delta) = \frac{1}{4} \csc(2\psi) (6\delta^2 \cos(2\psi) + (\delta^2 - 1) \cos(4\psi) + 3\delta^2 - 4\delta \sin(2\psi) + 1) \quad (55)$$

$$\beta_{0II}(\psi, \delta) = \frac{1}{2} \sec^2(\psi) ((\delta \cot(\psi) - 1)^2 - 2 \cos^2(\psi) \cot^2(\psi) (\sin(\psi) - \delta \cos(\psi))^2 + \cos(2\psi)) \quad (56)$$

$$\beta_{0III}(\psi, \delta) = \frac{1}{2} (\delta^2 - 2\delta \tan(\psi) + 1) \quad (57)$$

VIII. ACKNOWLEDGMENTS

This work was supported by Grant No. DEC-2013/11/B/ST3/04247 of the National Science Centre in Poland.

-
- [1] J.-R. Gong and L.-J. Wan, *J. Phys. Chem. B* **109**, 18733 (2005).
- [2] Z. Matharu, A. J. Bandodkar, V. Gupta, and B. D. Malhotra, *Chem Soc Rev.* **7;41(3)** 1363 (2012).
- [3] L. Niu, M. R. Lutfor, Y. Yang, and C. Wang, *J. Nanosci Nanotechnol.* **10** 7271 (2010).
- [4] Y. Li, J. Asik, Y. Yang, M. L. Rahman, X. Fan, and C. Wang, *J. Nanosci Nanotechnol.* **9(2)**, 1169 (2009).
- [5] W. Iglesias, T.J. Smith, P. B. Basnet, S. Stefanovic, C. Tschierske, D.J. Lacks, A. Jákli, and E.K. Mann, *Liquid Crystals* **431**, 141 (2012).
- [6] M. Banno, Z.-Q. Wu, K. Nagai, S.-I Sakurai, K. Okoshi, and E. Yashima, *Macromolecules* **43**, 6553 (2010).
- [7] L.-S. Li, J. Walda, L. Manna, and A. P. Alivisatos, *Nano Lett.* **2**, 557 (2002).
- [8] C. Querner, M. D. Fischbein, P. A. Heiney, and M. Drndić, *Adv. Mat.* **20**, 2308 (2008) (and references therein).
- [9] A. Jákli, *Liq. Cryst. Rev.* **1**,65 (2013).
- [10] H. Takezoe and Y. Takanishi, *Jap. J. of App. Phys.* **45**, 597 (2006).

- [11] V. Borshch, Y.-K. Kim, J. Xiang, M. Gao, A. Jákli, V. P. Panov, J. K. Vij, C. T. Imrie, M. G. Tamba, G. H. Mehl, and O. D. Lavrentovich, *Nature Communications* **4**, 2635 (2013).
- [12] D. Chen, J. H. Porada, J. B. Hooper, A. Klittnick, Y. Shen, M. R. Tuchband, E. Korblova, D. Bedrov, D. M. Walba, A. Glaser, J. E. MacLennan, and N. A. Clark, *PNAS* **110**, 15931 (2013).
- [13] M. G. Tamba, S. H. Salili, G. Zhang, A. Jakli, G. H. Mehl, R. Stannarius, and A. Eremin, *RSC Adv.* **5**, 11207 (2015).
- [14] O. Francescangeli, F. Vita, and E. T. Samulski, *Soft Matter* **10**, 7685 (2014).
- [15] P. Grzybowski and L. Longa, *Phys. Rev. Lett.* **107**, 027802 (2011).
- [16] T. Lubensky, *Phys. Rev. E* **66**, 031704 (2002).
- [17] a) L. Longa, G. Pająk, T. Wydro, *Phys. Rev. E* **79**, 040701(R) (2009); b) K. Trojanowski, G. Pająk, L. Longa and T. Wydro, *Phys. Rev. E* **86**, 011704 (2012); c) L. Longa and K. Trojanowski, *Acta Phys. Pol.* **44**, 1201 (2013).
- [18] H. Kunz, G. Zumbach, *Phys. Rev. B*, **46**, 662 (1992).
- [19] D. Frenkel and R. Eppenga, *Phys. Rev. A* **31**, 1776 (1985).
- [20] R. L. Vink, *Eur. Phys. J. B*, **72**, 225 (2009).
- [21] M. A. Bates and D. Frenkel, *J. Chem. Phys.* **112**, 10034 (2000).
- [22] R. Tavarone, P. Charbonneau, and H. Stark, *J. Chem. Phys.* **143**, 114505 (2015).
- [23] A. Chrzanowska, *Acta Physica Polonica B* **36**, 3163 (2005); **44**, 91 (2013).
- [24] F. Bisi, R. Rosso, E. G. Virga and G. E. Durand, *Phys. Rev. E* **78**, 011705 (2008).
- [25] J. A. Martínez-González, S. Varga, P. Gurin and J. Quintana-H., *EPL* **97**, 26004 (2012).
- [26] J. A. Martínez-González, S. Varga, P. Gurin and J. Quintana-H., *Journ. Mol. Liq.* **185**, 26 (2013).
- [27] Y. Martinez-Ratón, E. Velasco and L. Mederos, *Phys. Rev. E* **72**, 031703 (2005).
- [28] S. Varga, P. Gurin, J. C. Armas-Perez and J. Quintana-H., *J. Chem. Phys.* **131**, 184901 (2009).
- [29] R. Evans, *Adv. Phys.* **28**, 143 (1979).
- [30] J. D. Parsons, *Phys. Rev. A* **19**, 1225 (1979);
- [31] S. D. Lee, *J. Chem. Phys.* **87**, 4972 (1987); **89**, 7036 (1988).
- [32] Sz. Varga and I. Szalai, *Mol. Phys.* **95**, 515 (1998); *J. Mol. Liq.* **85**, 11 (2000).
- [33] R. B. Meyer, *Structural problems in liquid crystal physics. Les Houches Summer School in Theoretical Physics, 1973. Molecular Fluids*, eds Balian R, Weil G, 273 (Gordon and Breach,

New York, 1976).

[34] I. Dozov, Europhys. Lett. **56**, 247 (2001).

[35] L. Longa, P. Grzybowski, S. Romano and E. Virga, Phys. Rev. E **71**, 051714 (2005).